Controlling cell–cell interactions using surface acoustic waves

Feng Guo[a,1], Peng Li[a,1], Jarrod B. French[b,2], Zhangming Mao[a], Hong Zhao[b], Sixing Li[c], Nitesh Nama[a], James R. Fick[d], Stephen J. Benkovic[b,3], and Tony Jun Huang[a,3]

[a]Department of Engineering Science and Mechanics, The Pennsylvania State University, University Park, PA 16802; [b]Department of Chemistry, The Pennsylvania State University, University Park, PA 16802; [c]The Molecular, Cellular and Integrative Biosciences (MCIBS) Graduate Program, The Huck Institutes of the Life Sciences, The Pennsylvania State University, University Park, PA 16802; and [d]Medical School, Penn State Hershey Medical Group, Penn State Hershey Neurosurgery, State College, PA 16802

Contributed by Stephen J. Benkovic, November 20, 2014 (sent for review August 21, 2014)

The interactions between pairs of cells and within multicellular assemblies are critical to many biological processes such as intercellular communication, tissue and organ formation, immunological reactions, and cancer metastasis. The ability to precisely control the position of cells relative to one another and within larger cellular assemblies will enable the investigation and characterization of phenomena not currently accessible by conventional in vitro methods. We present a versatile surface acoustic wave technique that is capable of controlling the intercellular distance and spatial arrangement of cells with micrometer level resolution. This technique is, to our knowledge, among the first of its kind to marry high precision and high throughput into a single extremely versatile and wholly biocompatible technology. We demonstrated the capabilities of the system to precisely control intercellular distance, assemble cells with defined geometries, maintain cellular assemblies in suspension, and translate these suspended assemblies to adherent states, all in a contactless, biocompatible manner. As an example of the power of this system, this technology was used to quantitatively investigate the gap junctional intercellular communication in several homotypic and heterotypic populations by visualizing the transfer of fluorescent dye between cells.

cell–cell interaction | intercellular communication | surface acoustic waves | acoustic tweezers | acoustofluidics

Multicellular systems rely on the interaction between cells to coordinate cell signaling and regulate cell functions. Understanding the mechanism and process of cell–cell interaction is critical to many physiological and pathological processes, such as embryogenesis, differentiation, cancer metastasis, immunological interactions, and diabetes (1–3). Despite significant advances in this field, to further understand how cells interact and communicate with each other, a robust, biocompatible method to precisely control the spatial and temporal association of cells and to create defined cellular assemblies is urgently needed (4). Although several methods have been used to pattern cells, limitations still exist for the demonstrated methods including those that make use of optical, electrical, magnetic, hydrodynamic, and contact printing technologies (5–9). Firstly, most of the methods require modification of the cell's native state. The magnetic assembly method, for example, requires cells to be labeled with magnetic probes. Dielectrophoresis typically requires the use of a special medium (e.g., nonconductive) which may lack essential nutrients or have biophysical properties (such as the osmolality) that may adversely affect cell growth or physiology (6). Optical tweezers provide a label-free and contactless approach, but typically require high laser power to manipulate cells, leading to a high risk of cell damage (5). Secondly, the working principles of the existing technologies mostly preclude the combination of high precision and high throughput into a single device. It is difficult for high-throughput methods (such as magnetic assemblies) to achieve single-cell level precision, whereas the high-precision methods often require complex experimental setup to manipulate multiple cells simultaneously. Thirdly, most of the existing methodologies lack the ability to maintain cell assemblies in suspension, thereby limiting the application of these methods for the study of cell–cell and cell–matrix interactions.

As an alternative to using optical, electrical, or magnetic forces to manipulate cells, it has been demonstrated that biological specimens can also be manipulated using acoustic forces (10–16). Acoustic force can be applied through either bulk acoustic waves (BAWs) or surface acoustic waves (SAWs). Compared with the conventional BAW-based approaches (12, 13), SAW-based approaches (14–16) are becoming increasingly important in applications in cell biology and medicine as SAWs allow simpler device fabrication and experimental setup, higher manipulation resolution and flexibility, and better compatibility with optical imaging systems (allowing use of transparent devices). Thus far, the SAW-based approach has been reported to be able to manipulate single cells (15), but it has not yet been demonstrated for controlling cell–cell distance and interactions. This is mainly due to the difficulties in achieving a sufficient level of regulation of pressure nodes, which is needed to control the position of the cells with a high degree of precision. In this study, we demonstrate a SAW device that can accurately and reproducibly control pressure nodes and perform various functions for cell–cell interaction studies. Through superposing two orthogonal standing SAWs with differential input frequencies, we achieved highly regulated dot-array configuration of pressure nodes that facilitate high-precision control of cell–cell interactions, rather than the net-array pressure node configurations used in previous SAW devices (14, 15). This acoustic tweezers cell-manipulation method does not require any modification of

Significance

We present a unique acoustic well approach that can precisely control cell-to-cell distance and cell–cell interactions. Our technology can achieve high precision and high throughput simultaneously while preserving the integrity of cells. It is capable of creating cell assemblies with precise spatial control both in suspension and on a substrate. We envision the exploitation of this powerful technology, for example, in the study of cell–cell interactions in fields, such as immunology, developmental biology, neuroscience, and cancer metastasis, and in the studies of cell–cell and cell–matrix adhesion.

Author contributions: F.G., P.L., S.J.B., and T.J.H. designed research; F.G., P.L., Z.M., H.Z., and S.L. performed research; F.G., P.L., J.B.F., N.N., J.R.F., S.J.B., and T.J.H. analyzed data; and F.G., P.L., J.B.F., J.R.F., S.J.B., and T.J.H. wrote the paper.

The authors declare no conflict of interest.

[1]F.G. and P.L. contributed equally to this work.

[2]Present address: Department of Biochemistry and Cell Biology and Department of Chemistry, Stony Brook University, Stony Brook, NY 11794.

[3]To whom correspondence may be addressed. Email: sjb1@psu.edu or junhuang@psu.edu.

This article contains supporting information online at www.pnas.org/lookup/suppl/doi:10.1073/pnas.1422068112/-/DCSupplemental.

the growth conditions, allowing cells to be cultured in their native media. It is highly adaptable to the requirements of various applications and is capable of delivering both high precision (controlling intercellular distance at the micrometer scale) and high throughput (forming thousands of cell assemblies with tunable geometric configurations) in a single device. In addition, our method offers unprecedented flexibility over the control of cell assemblies. The geometry of cell assemblies can be finely tuned by changing the acoustic field. Moreover, the system is capable of holding cell assemblies in suspension at precise locations while assessing their biological functions without the use of permanent structures. These suspended cell assemblies can be allowed to settle to the surface to adhere and disperse. To demonstrate the power of this technology, we applied the system to explore gap junctional intercellular communication (GJIC) and quantitatively investigated various forms of functional intercellular communication by visualizing gap junctional dye exchange among coupled cells.

Results

Working Mechanism of the Tunable Acoustic Well. To develop a SAW device that is able to control both cell–cell distance and cell arrangement requires the formation of isolated pressure nodes with tunable pressure gradients. Thus, we established a dot-array configuration of pressure nodes by manipulating two orthogonal standing SAWs with slightly different frequencies (Fig. S1 and Movie S1, if with same frequency, Movie S2). When two orthogonal interdigital transducer (IDTs) pairs are deposited onto a 128° Y cut lithium niobate ($LiNbO_3$) piezoelectric substrate with a 45° angle to the *X* direction, they will share the same resonance frequency pattern (Fig. S2). The generation of two overlapping orthogonal standing SAWs relies upon different input resonance frequencies for different IDT pairs. Fig. 1 *A* and *B* shows the schematic and actual setup of the device, respectively.

A 6 × 6-mm^2 polydimethylsiloxane square chamber is bonded to a $LiNbO_3$ piezoelectric substrate at the middle of two orthogonal pairs of IDTs. The IDTs in our experiment have a combination of 40 pairs of electrodes that have a width and spacing gap of 75 μm. To ensure that the standing acoustic field is uniform throughout the chamber, the acoustic aperture is designed to be 9 mm in both directions. Each pair of IDTs is independently connected to a radiofrequency (RF) signal source to generate SAWs with different frequencies. Once the input signals are applied, square-shaped pressure node dot arrays will form on the substrate. Those standing SAWs leak and establish a differential acoustic potential field to the adjacent fluid medium (Fig. S3); this 3D acoustic field above each 2D square pressure node can function as an "acoustic well" (Fig. 1*C*). Simulations (Note S1) indicate that the superposition of the orthogonal standing SAWs creates isolated half-wavelength–sized square pressure nodes (Fig. 1*D*; arrows represent the direction of the radiation force). Cells can be manipulated in each acoustic well using the combination of acoustic radiation force and drag force driven by acoustic streaming. By modulating two input RF signals, we can precisely activate and tune the position and dimension of the acoustic well. As a result, a cluster of cells in a tunable acoustic well can be precisely manipulated. Cells trapped in this fashion can be made to form cell assemblies with controllable cell number, orientation, and configuration.

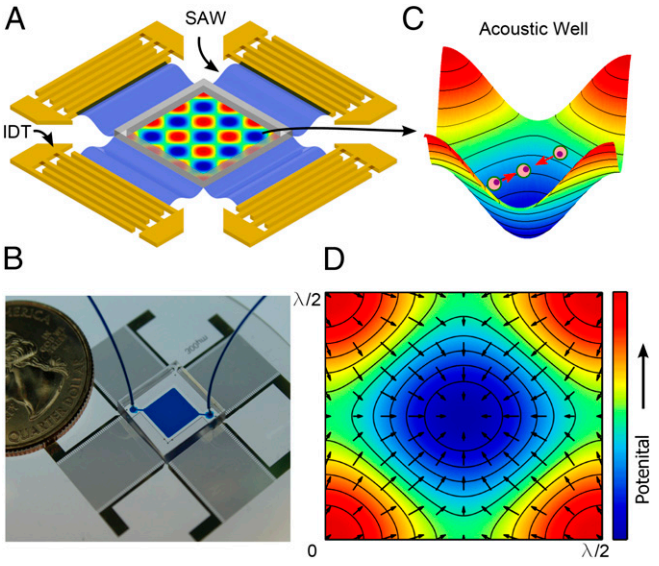

Fig. 1. Schematic of "tunable acoustic well." (*A*) Illustration of the experimental setup. (*B*) An image of the device. (*C*) Illustration of the function of the acoustic well. The pressure gradient causes the cells to be pushed into the middle of the pressure node. (*D*) Simulation result of the acoustic potential distribution in an acoustic well. The arrows show the direction of the radiation force.

Manipulation of Intercellular Distance. Once the array of pressure nodes is established as described in the previous section, tuning the intercellular distance of two cells becomes possible. When two cells are located within a unit square of the pressure antinode lattice (150-μm × 150-μm area), both of them will be pushed toward the same point (central pressure node). Thus, by controlling the movement toward the pressure node, the distance between two cells can be controlled. To achieve precise control of intercellular distance, the movement of cells must be stopped immediately upon regulation of the acoustic field. We first tested this process with 10-μm polystyrene beads. To attain a greater degree of control, particles were first arranged in lines with random distance along the lines by activating one pair of IDTs, thus creating standing waves aligned in one direction only. Once particles were stable, we applied a modulated RF signal in the orthogonal direction by activating the orthogonal pair of IDTs to push particles toward one another. The modulated signal was set to a pulse signal with 0.5-s duration and 2-s interval. The whole process was recorded (Movie S3) and analyzed to study the movement process (Fig. S4). When plotted, the pattern of movement showed a clear step-like shape that matched the period of the modulated input signal. The results indicate that the movement of particles is fully controlled by the input signals. This demonstrates the feasibility of using this acoustic method to tune the distance between two objects with micrometer-level resolution (Fig. S4). Therefore, it is feasible to use the acoustic well to control the intercellular distance of suspension cells.

We further examined if this method allows us to distinguish between two distinct states, direct contact and noncontact with a small distance, in the context of forming cell–cell contact for intercellular communication studies (17, 18). GJIC requires direct contact between cells, whereas communication that relies upon soluble factors is highly dependent upon the distance between the cells sending and receiving the signals. The generation of these two states is important to isolate effects from the two types of intercellular communication. Fig. 2*A* demonstrates that the distance between cells can be controlled using the same manner described above. The smallest movement step can be as small as ∼0.9 μm. Fig. 2*B* shows two HEK 293T cells with different desired intercellular distances of 15, 10, 5, and 0 μm, respectively. We then probed functional gap junctional communication with an assay using a membrane impermeable fluorescent dye, Calcein-AM. After cells were moved to the desired position, the SAW field was removed and cells were maintained in cell culture medium at 37 °C and 5% CO_2 environment. Fig. 2*C* shows that when the cells are in direct contact, fluorescent dye can be transferred to the neighboring cell after 1 h, indicating the formation of functional gap junctions. When cells were separated by a distance

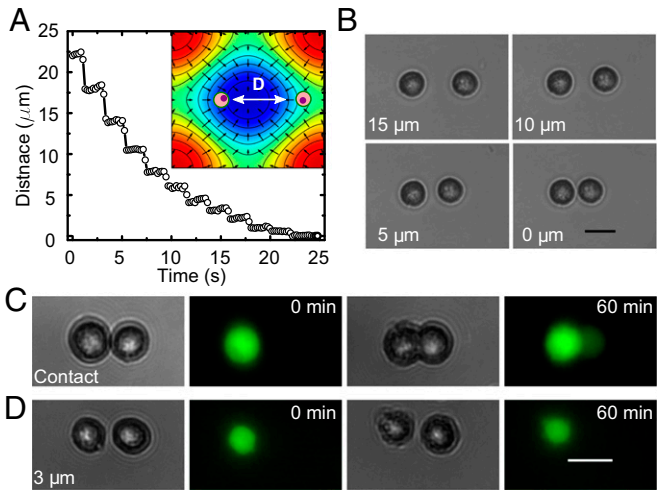

Fig. 2. Control of intercellular distances using acoustic wells. (*A*) The dependence of cell–cell distance on the input signals. A pulse signal (500-ms duration and 2-s interval) was applied to control the intercellular distance. (*B*) Using the tunable acoustic well, two HEK 293T cells are positioned with varied intercellular distances, 15, 10, 5, and 0 μm, respectively. (*C*) Two HEK 293T cells in contact with one another and visible dye transfer after 60 min. (*D*) Two HEK 293T cells were positioned with a distance of 3 μm. Dye transfer between the two cells is not observed after 60 min. Scale bar: 20 μm.

of 3 μm, no transfer of dye was observed after the same time interval (Fig. 2*D*). It should be noted that, depending upon their initial positions, separated cells may be moved out of their original positions in the current experimental setup due to evaporation-induced fluid instability.

Next, we performed statistical analysis of 139 cell pairs to study the dependence of cell contact formation on initial distance. After 30 min on-chip incubation, cell–cell contact formation probability was observed to increase with shorter intercellular distance (Fig. S5). The cell pair group with 0–3-μm intercellular distance has a probability of cell–cell contact formation of 73%, whereas the cell pair group with 9–15-μm initial intercellular distance forms junctions with a probability of 13%. The results indicated that the control of cell initial distance is able to generate the two types of intercellular communication under current experimental conditions. However, for applications where long-term, precise control of intercellular distance is critical, additional measures need to be taken to minimize the effects of flow instability on intercellular distance.

Formation of Suspended Cell Assembly. In addition to enabling the control of intercellular distance, the well-defined acoustic pressure nodes created by this device are also suitable for manipulating a group of cells to form different geometric configurations. When a group of cells are present within the confines of an acoustic well, they can be manipulated in concert and assembled into defined patterns using the acoustic radiation force. The acoustic well is highly tunable in terms of size and shape as indicated in both simulation and experimental results (Fig. 3 *A–D* and Movie S4). When we applied different input powers and frequencies (10 mW and 13.45 MHz; 30 mW and 13.35 MHz, respectively) to the two orthogonal IDT pairs, a rectangular-shaped acoustic well was generated (Fig. 3*A*). Using rectangular acoustic wells, cell chains with a cell number of two, three, and four can be formed by controlling the concentration of HeLa cells loaded into the device (Fig. 3 *E–H*). The direction of the rectangular acoustic well can also be reoriented by 90° (Fig. 3*B* and Movie S4) by switching the input powers of the two pairs of IDTs (30 mW and 13.45 MHz; 10 mW and 13.35 MHz, respectively). Similarly, when the same amplitude (20 mW) was applied in both directions, a square-shaped acoustic well could be formed (Fig. 3 *C* and *D*). In this case, cells in the acoustic well were assembled as a single-layer cluster (Fig. 3 *I–K*). It is also possible to shrink the size of the acoustic well (Fig. 3*D*) by increasing the input power (30 mW), forming 3D cell spheres as a result (Fig. 3*L*).

Formation of Gap Junctional Coupling. Our SAW device can be used to initiate and investigate GJIC. To examine whether HEK 293T cells can form functional gap junction channels in suspension state, a mixture of Calcein-AM stained cells and unstained cells was patterned into linear arrays and maintained in culture medium for the entire duration of the experimental period with the acoustic field (Fig. 4*A*). After 30 min of initial incubation, vivid dye coupling from donor cells to recipient cells can be observed in all of the linear arrays regardless of cell number. As expected, the larger the cell numbers, the longer it takes to observe evident dye coupling at the terminal cells (Fig. 4 *B–D*). If the cells are patterned in a linear array, their communication (as observed by the transfer of dye) occurs linearly. If cells are patterned in a cluster, their communication format will be changed as well. As shown in Fig. 4*E*, after tuning the acoustic well to assemble cells into a cluster, multiple cells receive the signal simultaneously from the donor cell. As a control, we used the gap junction inhibitor 18 α-glycyrrhetinic acid to block gap junction transfer. The inhibitor significantly reduces the dye coupling under our experimental conditions (Fig. S6). Collectively, these data demonstrate that HEK 293T cells can form functional gap junction channels in suspension, without the need for adhesion to a substrate. This platform for the acoustic manipulation of cells provides a simple and rapid way to examine the formation and function of GJIC in suspended cultures. Moreover, this technology is capable of controlling the patterns of cells, enabling the study of intercellular communication within groups of cells with varied architectures (e.g., linear vs. sphere).

Maintenance of Suspended Cell Assemblies and Translation to Adherent State. As discussed in the previous section, cells can be held at a stable distance above the substrate when an acoustic field is present, so it is possible to maintain assembled cells in the chamber without contacting the surface. The surface is thus free to be modified to facilitate cell attachment. As a result, cell–cell interaction and cell–matrix interaction can be studied either

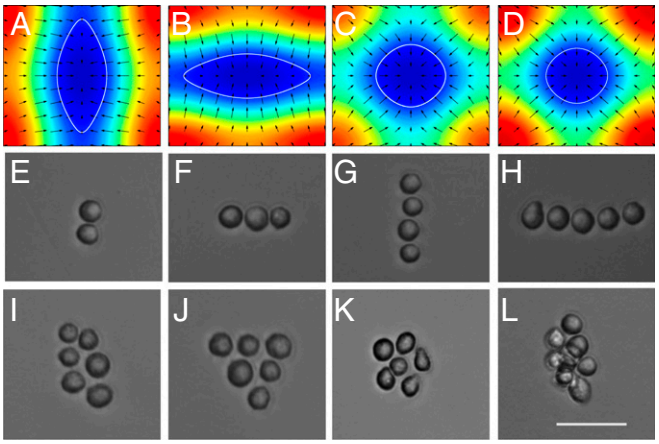

Fig. 3. Formation of cell assemblies with different geometries. (*A–D*) Simulation results of acoustic potential distribution in an acoustic well with different acoustic amplitudes. The white line indicates an acoustic potential with the same magnitude. (*E–H*) Linear shape of HeLa cell assemblies when applying linear-shaped acoustic wells. (*I–K*) Single-layer and (*L*) spherical shape of cell assemblies obtained when applying spherically shaped acoustic wells. Scale bar: 50 μm.

separately or sequentially in this device. To demonstrate this feature, we first created a linear pattern of HEK 293T cells using the method outlined above (Fig. 5*A*). When the SAW is present, the linear cell assembly is maintained in suspension for 1 h because of the combination of acoustic radiation force and acoustic streaming induced hydrodynamic force. During this period, only cell–cell adhesion occurs, despite the presence of a receptive surface that had been coated with collagen to facilitate cell attachment. After 1 h the SAW was removed, which allowed the cells to drop to the surface and attach to form a cell–matrix interaction. After another 40 min, HEK 293T cells first adhered to the surface and expanded their morphology along the surface (Fig. 5*B*).

After assembling cells in suspension, the geometric configuration of cell assemblies can also be translated to the surface as cells become adherent. To exploit the capability of this method for the study of intercellular communication under adherent conditions, we investigate the distinct gap junctional coupling properties of hTERT-HMVEC (human microvascular endothelial cells, CRL-4205) and HeLa S3 (CCL-2.2) cell lines. Endothelial cells are known to express gap junction proteins (e.g., Connexin 43) and allow small molecules to pass through the gap junction channels (19). A mixture of Calcein-AM stained and unstained HMVEC cells was patterned into linear assemblies under the SAW field as described in the previous section. Once the linear pattern was stable, the SAW field was removed to allow cells to settle down and attach to the surface. HMVEC cells started to attach and spread 25 min after settling down, whereas the geometric configuration of the cell assembly was well maintained (Fig. 5*C*). After all of the cells became adherent to the substrate, significant dye transfer was occurring from stained (donor) cells to unstained (recipient) cells within 40 min (Fig. 5*D*). In contrast, the HeLa cell line does not express connexin proteins, essential components of gap junction channels, and therefore lacks the ability to exhibit dye transfer (20). As shown in Fig. 5*E*, HeLa S3 cells showed similar attachment and spread dynamics after patterning in suspension. However, dye coupling between adherent HeLa S3 cells was not observed even 2 h after they became completely adherent (Fig. 5*F*).

Quantitative Evaluation of GJIC. As demonstrated in the previous sections, the acoustic well allows flexible cell assembly with high-precision spatial control. Here we used GJIC as an example to illustrate that our technology offers unprecedented precision and versatility for quantitative intercellular communication studies. In particular, we used a preloading assay to evaluate the gap junctional dye transfer dynamics. Preloading assays allow for minimal disruption of cell integrity and normal physiology by avoiding microinjection and high-power laser irradiation. However, conventional preloading assays are not suitable to study the dynamics of dye transfer with high temporal resolution due to the inability to control the beginning of cell–cell contacts and the geometry of cell assemblies (21). With the assistance of acoustic wells, we are able to interrogate early dye transfer dynamics using a preloading assay. In addition, the differences in dye transfer dynamics between the suspension and adhesion states of cells can be studied using the acoustic well. In this section, we demonstrate two unique features of our acoustic well technology: (*i*) the capability to quantitatively interrogate very early dye transfer dynamics of cell assemblies (homotypic or heterotypic cell assemblies); and (*ii*) the capability to hold cell assemblies in suspension at precise locations while quantitatively assessing their biological functions.

We first studied dye transfer dynamics of adherent cells with different cell configurations (both homotypic and heterotypic cell pairs). We chose an endothelial (HMVEC) and a glioma cell line (U87) as our model. It has been widely reported that the process of angiogenesis in glioma is very active and there are strong interactions between glioma cells and endothelial cells via either soluble factors or gap junction-based communication (22). After assembling cell pairs using the acoustic well, the dye transfer dynamics of endothelial cell pairs, glioma cell pairs, and endothelial and glioma cell pairs was recorded (Fig. S7 *A*–*C*), analyzed, and plotted (Fig. 6 *A*–*C*), respectively. By calculating the intensity plots using Fick's equation (23) (see details in Note S2),

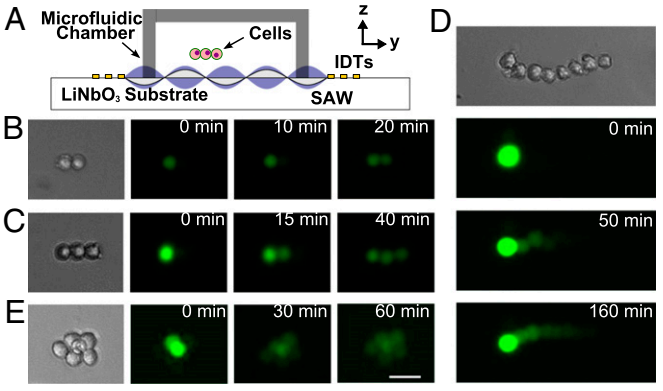

Fig. 4. Dye coupling between HEK 293T cells with defined arrangement. (*A*) Schematic of experimental setup. (*B*) Bright-field image and time-lapse fluorescence images of cell pair, (*C*) a three-cell system, (*D*) a linear cell assembly, and (*E*) a 2D, multiple-cell system trapped within a well-controlled acoustic field. The dye transfer between the cell assemblies can be observed over time. (*B*–*D*) The dye molecules transferred sequentially because of the defined linear assembly. (*D* and *E*) Different from the linear cell assemblies, the spherical cell assembly allows dye transfer to occur with all neighboring cells simultaneously. Scale bar: 50 μm.

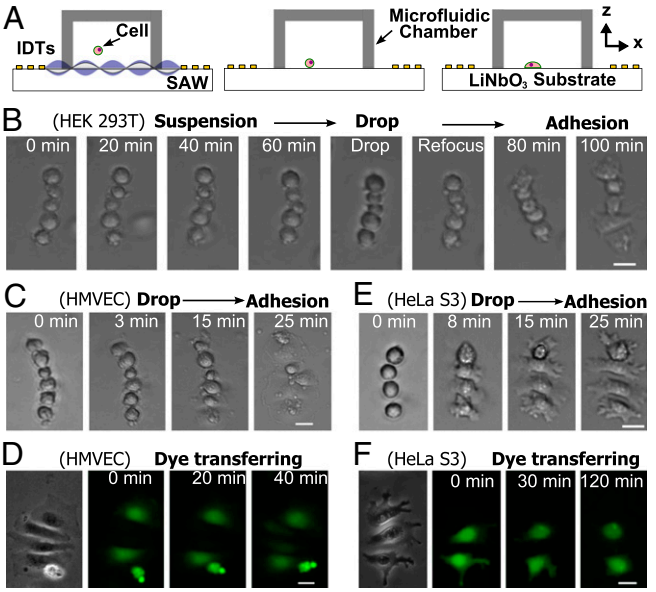

Fig. 5. Translation of suspended assemblies to the adherent state. (*A*) Schematic of experimental setup and procedure. Linear assemblies of cells were formed under the control of a tunable acoustic well. After the removal of the acoustic field, cells were allowed to drop to the surface and attach. (*B*) The process of in-suspension assembly and attachment. HEK 293T cells were first assembled in suspension. The acoustic field was maintained for 1 h in order that cells could be kept in suspension regardless of the properties of the surface. Once the acoustic field is removed, cells quickly attach to the collagen-coated surface and start to spread while maintaining the same assembly as in suspension. In-suspension assembly and attachment of (*C*) HMVEC and (*E*) HeLa S3 cells, respectively. Dye transfer between attached (*D*) HMVEC and (*F*) HeLa S3 cells, respectively, with defined geometry. Scale bar: 20 μm.

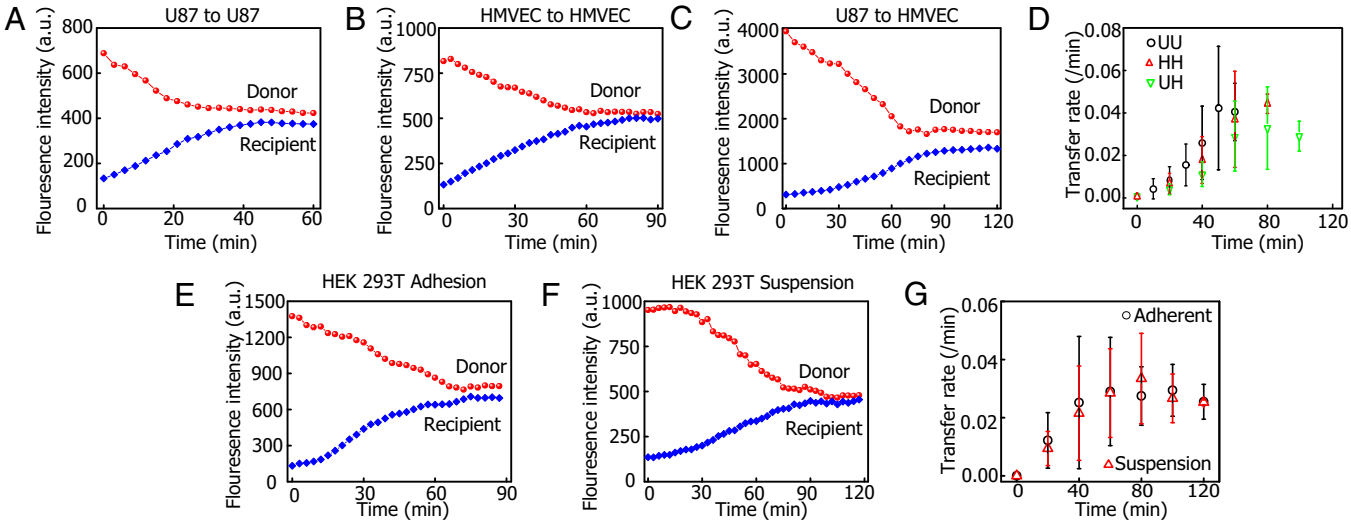

Fig. 6. Quantitative comparisons of gap junctional dye transfer between homotypic and heterotypic cell pairs, and between adherent and suspended cell pairs. (*A*–*C*) Fluorescence intensity plots over time for U87 to U87, HMVEC to HMVEC, and U87 to HMVEC cell pairs, respectively. (*D*) Dye transfer rates at different time periods for the three types of cell pairs. (*E* and *F*) Fluorescence intensity plots over time for adherent and suspension cell pairs, respectively. (*G*) Dye transfer rates at different time periods for the two types of cell pairs. Error bars represent the SD of multiple cell pairs ($n = 20$). These rates are for 20-min (or 10-min) intervals ending at the time shown on the *x* axis.

transfer rates of different time points can be obtained. Fig. 6*D* shows that the average dye transfer rates at each time intervals for all three types of cell pairs change over time. At the early time points (0–20 min), the transfer rates are slower than the later stages. The trend of transfer rate is different from what has been previously reported from local activation of molecular fluorescent probe experiments, which showed consistent dye transfer constant over the time period (23). The reason lies in that the acoustic well experiments enable the examination of dye transfer immediately after cell–cell contacts. As a result, very early dye transfer dynamics can be captured during which the gap junction channels are still forming. Conventionally, gap junctional dye transfer is often studied when channels have already reached equilibrium due to the inability to control the starting point of cell–cell contact. At later stages (after 60 min), the transfer rates of the three type cell pairs tend to be consistent, indicating that the formation of gap junction channels approaches equilibrium. When comparing the transfer rates at late stages for the three configurations, U87 to U87 pairs are similar to HMVEC to HMVEC pairs ($0.040\ \text{min}^{-1} \pm 0.013\ \text{min}^{-1}$ vs. $0.044\ \text{min}^{-1} \pm 0.005\ \text{min}^{-1}$). Both of the transfer rates are faster than the heterotypic cell pair U87 to HMVEC ($0.029\ \text{min}^{-1} \pm 0.007\ \text{min}^{-1}$). In addition to comparing dye transfer rates when they are in the stable stage, we also calculated the time that is needed for the dye transfer to reach equilibrium. For U87 to U87, HMVEC to HMVEC, and U87 to HMVEC pairs, the times are 58 ± 11 min, 67 ± 12 min, and 81 ± 23 min, respectively. The results indicated the same conclusion as using the dye transfer rates: dye transfer between the homotypic cell pairs is faster than the heterotypic cell pairs. The results are also consistent with the existing understanding that fewer junctions are formed when different cell types are coupling (24).

The acoustic well not only allows the comparison of gap junctional communication dynamics between different adherent cell pairs, but also enables the comparison of dye transfer dynamics between cells in suspension and adhesion states. We examined the dye transfer dynamics of HEK cells in both adhesion and suspension states. To maintain cells in suspension the acoustic field was maintained throughout the experiment. The fluorescence images of dye transfer between adhesion HEK 293T cell pairs and suspension HEK 293T cell pairs are shown in Fig. S7 *D* and *E*, respectively. By calculating the fluorescence intensity profile (Fig. 6 *E* and *F*) in the same way as the previous experiments, dye transfer rates of different time periods can be obtained (Fig. 6*G*). Fig. 6*G* shows that both adhesion pairs and suspension pairs have similar dye transfer dynamics. The time to reach equilibrium also showed no significant difference between adhesion and suspension HEK cell pairs (75 ± 25 min vs. 85 ± 25 min). The results suggest that cell adhesion has little impact on the overall rate of gap junctional dye transfer dynamics for HEK 293T cells. However, the effects of cell adhesion on dye transfer dynamics may vary for different cell types. It should also be noted that the large variance in the observed intercellular dye transfer among different cell pairs may be caused by the heterogeneity of cell populations and cell cycle states.

Discussion

We present a highly versatile tool for controlling the spatial arrangement of cultured cells through the use of tunable acoustic wells. Because the position and shape of acoustic wells can be precisely modified, our technology has the unique ability to form cellular arrangements with complex geometries, as well as to push the individual cells together with micrometer precision. In addition, the contactless, label-free nature and mild force amplitude allow the acoustic method to manipulate cells with a minimal level of disruption to the cells. We performed an RNA microarray test to examine the impact of SAWs on gene expression. The results indicate that there is no significant difference on gene expression between the control group and the SAW-treated group (Note S3 and Table S1). In this work, we demonstrated that the acoustic well is capable of performing multiple important tasks for intercellular communication studies. These tasks include the control of intercellular distance, the engineering of homotypic or heterotypic cell assemblies, the monitoring of the exchange of small molecules among suspended cells, and the transformation of cellular aggregates from suspended to adherent states and subsequent investigation of assembly and communication in adherent cells.

The ability to assemble and maintain cells in suspension with defined geometry is a unique feature of this acoustic tweezers system. In this work, we exploited this functionality to GJIC for adherent HEK 293T cells in suspension in a defined assembly, despite the fact that these cells normally are cultured as adherent

monolayers. Although this study demonstrates the power of the technology, it is only one demonstration of its use. This technology is ideally suited to investigate the mechanisms of cell–cell communication occurring within cells maintained in suspension. This capability has particular relevance to experiments performed upon neoplastic cells, as metastatic phenotypes are known to be associated with cellular morphologies such as aggregates, cell balls, or even single-cell chains that resemble cells maintained in suspension. Furthermore, neoplastic cells isolated from human body fluids such as blood, cerebral spinal fluid, pleural effusions, and peritoneal fluid typically have morphologies that differ from their tissue of origin and oftentimes resemble cells cultured in suspension (25).

This SAW-based method also enables the label-free study of the correlation between cell–cell adhesion and cell–matrix adhesion (for example, the cross-talk between cadherin and integrin) (26, 27). Current methods require surface modification to avoid integrin activation and use fibronectin-coated beads to trigger integrin to study the impacts on biomechanics (28) such as cell–cell adhesion. Using the acoustic well, cell–cell adhesion can be first induced in suspension, and after removal of the SAW field, cells will descend to the modified surface to activate integrin. This acoustic well technology was demonstrated to create cell assemblies in suspension that can be translated to patterns upon adhesion to the substrate. When cells initially attach and spread on the surface, the geometry can be maintained strictly. For cells that tend to migrate quickly, however, the geometry of the patterned cells may be disrupted after long-term cell culture. As a result, in some cases the acoustic assembly alone cannot replace the method of surface modification to precisely define the region of cell growth. However, this technology can be easily combined with surface modification methods or other approaches to enhance the efficiency of forming cell colonies. In addition, this feature makes the acoustic method very suitable to study cell migration as it avoids physical confinement introduced by surface modification while generating a defined geometry as a controllable starting point.

We have demonstrated how acoustic radiation forces can be exploited to generate a controllable motive force that can be used for high-precision fabrication and manipulation of cell assemblies. By modulating the gradient and position of pressure nodes within this device, we were able to precisely control the intercellular distance of cells cultured in suspension, to assemble cells with defined geometries, to maintain cellular assemblies in suspension, and to then convert these suspended assemblies to adherent states. The ability to precisely manipulate and pattern cells using the acoustic well provides a powerful tool for myriad investigations, particularly those that involve the study of intercellular communication. We expect that the implementation of this technology will significantly advance fields of study focused upon cell–cell interactions, such as immunology, developmental biology, neuroscience, and cancer metastasis.

Materials and Methods

Device Fabrication and Experiment Setup. The device was fabricated by bonding the PDMS based microchannels onto a lithium niobate ($LiNbO_3$) substrate coated with IDTs. Standard softlithography procedure was followed to make the PDMS device. IDTs on the $LiNbO_3$ substrate was created by standard photo lithography and lift-off processes. The detailed fabrication procedure was described previously (15). To generate the SSAW field, two pairs of IDTs were individually activated by a double-channel function generator and two amplifiers. The details of experiment setup can be found in Note S4.

Cell Culture in the SAW Device. For long-term on chip dye transfer observation, cells were maintained by a customized on-stage cell culture chamber at 37 °C and 5% CO_2 condition. Details on cell preparation and culture are available in Note S5.

Image Acquisition and Analysis. Images were acquired through an inverted microscope with a charge coupled device (CCD) camera, and analyzed with the ImageJ software package. Details on image acquisition and analysis can be found in Note S6.

ACKNOWLEDGMENTS. We thank Dr. Zhihao Jiang for SAW device characterization; Dr. Craig Praul, Yihan Li, and Dr. Debashis Ghosh and Penn State Genomics Core Facility for the microarray assay; and Dr. Yijun Deng, Dr. Xiaoyun Ding, Dr. Janos Vörös, and Dr. Vivek Kapur for fruitful discussions. We gratefully acknowledge financial support from the National Institutes of Health (1R33EB019785-01 and 1DP2OD007209-01), the National Science Foundation, and the Penn State Center for Nanoscale Science (Materials Research Science and Engineering Centers) under Grant DMR-0820404. J.B.F. acknowledges the Canadian Institutes of Health Research for Fellowship support.

1. Streuli CH, Bailey N, Bissell MJ (1991) Control of mammary epithelial differentiation: Basement membrane induces tissue-specific gene expression in the absence of cell-cell interaction and morphological polarity. *J Cell Biol* 115(5):1383–1395.
2. Manz BN, Groves JT (2010) Spatial organization and signal transduction at intercellular junctions. *Nat Rev Mol Cell Biol* 11(5):342–352.
3. Brownlee M (2001) Biochemistry and molecular cell biology of diabetic complications. *Nature* 414(6865):813–820.
4. Guo F, et al. (2013) Probing cell-cell communication with microfluidic devices. *Lab Chip* 13(16):3152–3162.
5. Zhang H, Liu K-K (2008) Optical tweezers for single cells. *J R Soc Interface* 5(24): 671–690.
6. Voldman J (2006) Electrical forces for microscale cell manipulation. *Annu Rev Biomed Eng* 8:425–454.
7. Pan Y, Du X, Zhao F, Xu B (2012) Magnetic nanoparticles for the manipulation of proteins and cells. *Chem Soc Rev* 41(7):2912–2942.
8. Suri S, et al. (2013) Microfluidic-based patterning of embryonic stem cells for in vitro development studies. *Lab Chip* 13(23):4617–4624.
9. Théry M (2010) Micropatterning as a tool to decipher cell morphogenesis and functions. *J Cell Sci* 123(Pt 24):4201–4213.
10. Bruus H, et al. (2011) Forthcoming Lab on a Chip tutorial series on acoustofluidics: Acoustofluidics-exploiting ultrasonic standing wave forces and acoustic streaming in microfluidic systems for cell and particle manipulation. *Lab Chip* 11(21):3579–3580.
11. Mulvana H, Cochran S, Hill M (2013) Ultrasound assisted particle and cell manipulation on-chip. *Adv Drug Deliv Rev* 65(11-12):1600–1610.
12. Bazou D, et al. (2006) Gap junctional intercellular communication and cytoskeletal organization in chondrocytes in suspension in an ultrasound trap. *Mol Membr Biol* 23(2):195–205.
13. Christakou AE, et al. (2013) Live cell imaging in a micro-array of acoustic traps facilitates quantification of natural killer cell heterogeneity. *Integr Biol (Camb)* 5(4): 712–719.
14. Shi J, et al. (2009) Acoustic tweezers: Patterning cells and microparticles using standing surface acoustic waves (SSAW). *Lab Chip* 9(20):2890–2895.
15. Ding X, et al. (2012) On-chip manipulation of single microparticles, cells, and organisms using surface acoustic waves. *Proc Natl Acad Sci USA* 109(28):11105–11109.
16. Ding X, et al. (2013) Surface acoustic wave microfluidics. *Lab Chip* 13(18):3626–3649.
17. Kholodenko BN (2006) Cell-signalling dynamics in time and space. *Nat Rev Mol Cell Biol* 7(3):165–176.
18. Ottone C, et al. (2014) Direct cell-cell contact with the vascular niche maintains quiescent neural stem cells. *Nat Cell Biol* 16(11):1045–1056.
19. Villars F, et al. (2002) Effect of HUVEC on human osteoprogenitor cell differentiation needs heterotypic gap junction communication. *Am J Physiol Cell Physiol* 282(4): C775–C785.
20. Elfgang C, et al. (1995) Specific permeability and selective formation of gap junction channels in connexin-transfected HeLa cells. *J Cell Biol* 129(3):805–817.
21. Abbaci M, Barberi-Heyob M, Blondel W, Guillemin F, Didelon J (2008) Advantages and limitations of commonly used methods to assay the molecular permeability of gap junctional intercellular communication. *Biotechniques* 45(1):33–62.
22. Zhang W, et al. (1999) Direct gap junction communication between malignant glioma cells and astrocytes. *Cancer Res* 59(8):1994–2003.
23. Dakin K, Zhao Y, Li WH (2005) LAMP, a new imaging assay of gap junctional communication unveils that Ca2+ influx inhibits cell coupling. *Nat Methods* 2(1):55–62.
24. Woodward TL, Sia MA, Blaschuk OW, Turner JD, Laird DW (1998) Deficient epithelial-fibroblast heterocellular gap junction communication can be overcome by co-culture with an intermediate cell type but not by E-cadherin transgene expression. *J Cell Sci* 111(Pt 23):3529–3539.
25. DeMay RM (2012) *The Art and Science of Cytopathology* (American Society for Clinical Pathology, Chicago), 2nd Ed, pp 291–292.
26. Borghi N, Lowndes M, Maruthamuthu V, Gardel ML, Nelson WJ (2010) Regulation of cell motile behavior by crosstalk between cadherin- and integrin-mediated adhesions. *Proc Natl Acad Sci USA* 107(30):13324–13329.
27. Fu J, et al. (2010) Mechanical regulation of cell function with geometrically modulated elastomeric substrates. *Nat Methods* 7(9):733–736.
28. Fletcher DA, Mullins RD (2010) Cell mechanics and the cytoskeleton. *Nature* 463(7280):485–492.